Design and Initial Testing of a High Speed 45 kW Switched Reluctance Drive for Aerospace Application

James Borg Bartolo, Marco Degano *Member, IEEE*, Jordi Espina and Chris Gerada *Member, IEEE*

***Abstract*—This paper presents innovative research towards the development of a 45 kW high speed switched reluctance drive as an alternative starter-generator for future aero-engines. To perform such a function the machine had to be designed with a very wide constant power-speed range. During engine-start/motoring mode, a peak torque demand of 54 Nm at 8 krpm was met, whilst in generating mode, 19.2-32 krpm, the machine was designed to deliver a constant power of 45 kW. The key enabling feature of the design lies in the novel rotor structure developed so as to allow for such a wide speed range. The results presented, are those measured during the initial testing phase and validate the system design and performance in the low-speed region with the machine operated in starting-mode. The measured machine power density is at 9.8 kW/ltr, whilst the global system efficiency is at 82%.**

***Index Terms*— Electric Machines, High speed generators, Reluctance Generators.**

I. INTRODUCTION

AIR travel has increased in popularity and scope, a trend which is likely to continue for years to come [1]. Such growth however, is taking place in a very demanding environment for both operators and component manufacturers, who struggle to lower operational/running costs and environmental impact, whilst at the same time increasing aircraft safety and reliability.

To meet such demands, a lot of effort is being put into the development of a More Electric Aircraft, encompassing a More Electric Engine [1, 2]. Both concepts express the need for placing electricity as the unitary vector of energy, over hydraulic and pneumatic methods, providing advantages in terms of: relative ease of power routing within the airframe, a reduction in both working-fluid volume and piping infrastructure, potentially lighter aircraft and an increase in global system efficiency and reliability through lower component count and spool speed decoupling.

Manuscript received December 14, 2015; revised May 16, 2016 and August 3, 2016; accepted August 22, 2016.

J. Borg-Bartolo was with the Power Electronics and Control Group at the University of Nottingham during the course of this work (e-mail: james.borg-bartolo@maxonmotor.com Phone: 0041 764274225.

M. Degano, J. Espina and C Gerada are with Power Electronics Machines and Control group (PEMC) at the University of Nottingham, University Park, Nottingham, NG72RD (e-mails: Marco.Degano@nottingham.ac.uk; Jordi.Espina@nottingham.ac.uk; Chistopher.Gerada@nottingham.ac.uk).

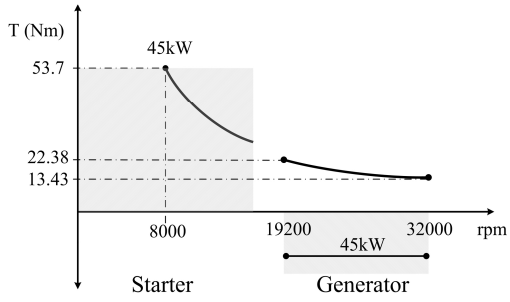

Fig.1. Typical Torque-speed requirements considered for the design of a modern starter-generator

Such a situation is thus bringing about an increased need for larger, more reliable, on-board generation systems [2].

In response to this, and following from earlier work presented in [3, 4] this paper details the work done in designing, building and testing of a new switched reluctance based starter/generator (S/G) system for a modern regional jet aero-engine; capable of satisfying the wide constant power speed range detailed in Fig.1.

Such a function requires the machine to initially act as a motor, spinning the aero-engine through the starting sequence, till light-off speed (maximum torque condition). It then continues to assist the engine till idle speed is reached, following which the machine acts as a generator, ref. Fig.1.

The machine presented, was designed to deliver its maximum torque of 53.8 Nm at 8 krpm, and will be required to supply a 45 kW load at shaft speeds up to 32 krpm.

An identical physical envelope to that imposed on current state-of-the art S/G machines was adopted such that the maximum permissible stator outer diameter was limited to 200 mm, and a shared oil system was considered, with an outer-jacket stator-cooling topology. The inlet oil temperature was specified at 120˚C.

Such an envelope was found to be in close agreement with what was previously reported in [5-7] for similar SR-based drives. However, in all of the mentioned cases the starting-power demand was much lower than that required during generating mode, resulting in a reported constant-power speed

range-ratio (CPSRR) which varied from 1:2 up to 1:3.25 [8]. The drive detailed in this work was required to achieve a CPSRR of 1:4, in discontinuous-conduction mode and thus presents a novelty to the field of SR based starter/generators rated at this power level.

Following this introduction, the present document is divided into three main parts. The first, section II, details the governing principles, and salient analysis performed in designing the novel switched-reluctance machine (SRM) capable of achieving the stated wide constant power speed range. The second part, in Sections III, IV and V, presents the built power electronic converter; adopted control strategy and test setup for initial machine testing. The third part of the paper, in section VI, presents the measured results obtained from initial testing of the assembled drive. Finally a number of conclusions are presented in section VII.

II. The Switched Reluctance Machine

The SRM is a doubly salient, singly excited machine. In its classical form, the machine presents itself with a 'simple' construction having a single element rotor and concentrated windings. These attributes coupled with diagnostic techniques such as those presented in [9], renders such a topology a favourite for high speed, harsh environment applications. The studied variant of this machine is of such classical type.

A number of stator and rotor pole number combinations were initially investigated. It was found however that the 6/4 pole combination provided the best compromise between iron losses, self-starting capability and torque ripple [5-7].

The presented design makes use of a novel, rotor pole chamfer, ref. section II D, which allows for the demanded wide constant power speed range to be achieved.

A. Basic operation and principles

Due to its sequential commutation, the electromechanical energy conversion in such machines occurs in discrete cycles, or strokes, through the interaction of one (or more), stator and rotor pole pairs.

The energy supplied to a model system formed by a set of current-carrying phase coils whose flux couples with, and induces a resultant force within a rotating element, can be summarized in terms of measurable (or easily derivable) quantities via conservation principles as:

$$i.d\psi = dw_s + T_e\, d\vartheta \tag{1}$$

Where: i is the current flowing into the system, ψ is the flux linkage, w_s is the total stored energy, T_e is the developed torque, and ϑ is the general rotor displacement.

In order to facilitate the initial treatise of the system, it is very useful to consider the flux linkage setup in a phase coil system as being a function of the currents flowing within it rather than vice versa, such that (1) can be restated in terms of the incremental change in co-energy W_f, for the single phase system by:

$$dW_f(i,\vartheta) = \psi(i,\vartheta)di + T_e\,(i,\vartheta)d\vartheta \tag{2}$$

Due to the cyclic nature of the energy conversion process undertaken, and considering steady state conditions, it can be shown that no net change in the energy level of the system occurs over one cycle, thus one can restate (2) in its integral form by:

$$\int_{C_{i\vartheta}} T_e(i,\vartheta)d\,\vartheta = -\int_{C_{i\vartheta}} \psi(i,\vartheta)di \tag{3}$$

Where: $C_{i\vartheta}$ is the path in the coordinate space i-ϑ. This relationship thus states that the developed torque during one cycle can be evaluated by taking the integral of the flux linkage locus in a diagnostic plane, ψ-i along the contour specified in the coordinate space i-ϑ, which in practice is none other than the time-domain current waveform imposed on the winding; thus highlighting the main advantage of using the co-energy principle in correlating measurable electrical terminal quantities to measureable mechanical effects.

Using standard differential theory and the co-energy expression given in (2) it can be shown that the torque developed under one pole can be stated in terms of the experienced rate-of-change of energy with respect to rotor positions as:

$$T_e(i,\theta_m) = \frac{\delta W_f(i,\theta_m)}{\delta\theta_m} \tag{4}$$

Where: $\delta\theta_m$ refers to the change in angular position during the imposed phase-conduction period θ_{cond} , and $\delta W_f(i,\theta_m)$ is the energy converted during such cycle, evaluated as the area enclosed by the flux-linkage locus in the ψ-i domain (one such locus was derived numerically in Fig.5).

By considering (4), the area enclosed by the flux-linkage locus in the ψ-i domain must therefore relate to the average developed torque per stroke such that:

$$W_f = T_{stroke}\cdot\theta_{cond} = \frac{T_{avg}\cdot 2\pi}{M} \tag{5}$$

Where: M is the number of strokes per mechanical cycle. Thus, knowing the value of the required average torque the machine should develop, the energy per cycle can be estimated. This, together with using a linear inductance model and a reluctance network approach allows for values flux linkage to be obtained at various rotor positions and hence an initial machine geometry to be estimated, as described in [3].

B. Electromagnetic design considerations

To meet the wide constant power-speed requirements set out in Fig.1, the two extreme power nodes were considered as design points.

The first, defined as the base-speed, was chosen at 8krpm (peak torque node), with initial machine sizing carried out at this point for a peak phase current of 600 A. Such an exercise was carried out during the earlier design stages, using an analytic method developed by the author, based on (4), (5) and work published in [10-14]. In summary, the proposed stator model adopted a linear approximation to the magnetic circuit,

assuming that only the stator poles are in heavy saturation [11]. Thus initial sizing relationships for the stator tooth arc angle βs, stator back iron b_{sy}, stator tooth width T_{sb} and bore Diameter D were derived. The rotor geometry-estimation-model was similarly based on a reluctance network approach [3]. A set of curves for the estimated flux linkage variation within the stator tooth, for a given MMF level, as a function of machine air-gap l_g and rotor chamfer angle θ_{cm} were derived [3]. Following this initial sizing exercise, an iterative optimization technique relying on finite element simulations was later used to tune the obtained dimensions and arrive to a final design for the required machine fulfilling the necessary base speed ratings.

The second design point considered was the high speed constant power node at 45 kW, 32 krpm. The operation of the base-speed-optimized machine at such high speed was verified, via analytical methods based on [15] and the required geometry optimization was carried out as detailed in [3] to meet requirements.

The final geometry for the optimized machine is given in Fig.2. It has a 120 mm bore diameter, with an air gap of 0.5 mm and a stack length of 150.6 mm; its outer diameter is 192 mm, and occupies a volume of 4.592 ltrs.

An overlapping current excitation was assumed throughout the design process. This, together with the implemented circumferentially-alternating pole distribution, allowed for a short flux-path during commutation to the neighbouring pole.

Both stator and rotor employed a cobalt-iron laminate material at 0.1 mm, post-process annealed at different conditions to reach optimal electromagnetic and mechanical properties respectively.

C. Stator design

The main feature in the stator design was the inclusion of the stator-pole tips, which allowed for a reduction in tooth width whilst ensuring that the minimum pole arc at the bore diameter βs, required for self-starting, is maintained. Whilst not being novel, this feature contributed towards reaching the required operating torque-speed envelope. By solely considering the low speed performance as a first iterate, a value of 0.49 was chosen for the pole envelope at the tooth-base "S_{penv}". However, during the high speed optimization process this value was reduced to 0.44 which allowed for a 3.4% increase in the high speed performance of the machine. Due to the incurred reduction in tooth-surface area, an earlier saturation of the machine was brought about, such that at low speed mode, a 2.8% reduction in torque was noted. As discussed by the author in [4] notwithstanding this reduction, the design still met the low speed requirement with a healthy margin as detailed in the coming sections.

D. The novel rotor structure

The terminal voltage equation of the SRM can be stated in terms of the flux linkage variation as:

$$v_t(i,\theta_m) = r_s i + \frac{d\psi(i,\theta_m)}{di}\frac{di}{dt} + \frac{d\psi(i,\theta_m)}{d\theta_m}\frac{d\theta_m}{dt} \qquad (6)$$

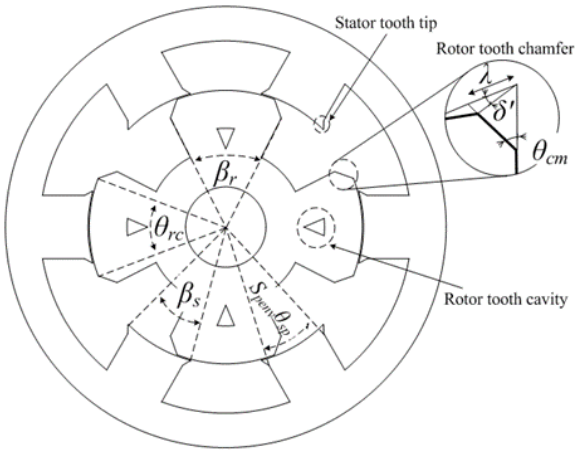

Fig.2. Design of SRM having a very wide constant power speed range

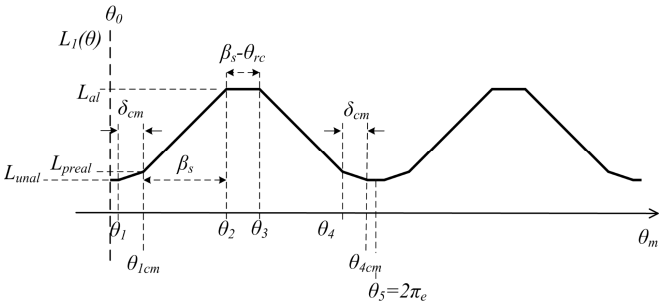

Fig.3. Ideal position inductance-variation for the linear machine with rotor pole chamfer

Where: v_t is the terminal voltage, r_s is the phase resistance, and $\psi(i,\theta_m)$ is the flux linkage variation as a function of current and rotor position θ_m. It can be noted that one of the major hindrances to developing the required torque at high speed values, for a fixed converter voltage, is the induced pseudo-Back EMF term (third term RHS) which reduces the available voltage ceiling and thus blocking the required current from being present in the winding.

By introducing a pole chamfer angle θ_{cm}, ref. Fig.2, a handle on such a term could thus be introduced.

1) Rotor Electromagnetic Design

During pole alignment the inductance increases in a proportional way to the stator pole-overlap, such that the maximum change-of-inductance is only limited by the magnetic state of the stator pole arc and its duration is dictated by βs.

By introducing a pole chamfer, the rotor crown arc angle θ_{rc} could be decoupled from βr such that a pre-alignment period could be defined by δ_{cm} , and expressed as:

$$\delta_{cm} = \beta_r - \theta_{rc} \qquad (7)$$

where: θ_{rc} is the rotor crown angle and βr is the conventional rotor pole arc angle.

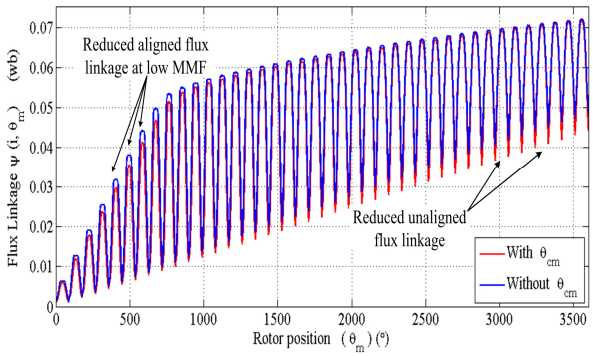

Fig.4. Plot showing the flux-linkage for the chamfered and non-chamfered designs. Current increased by 25A at each θ_{tp}

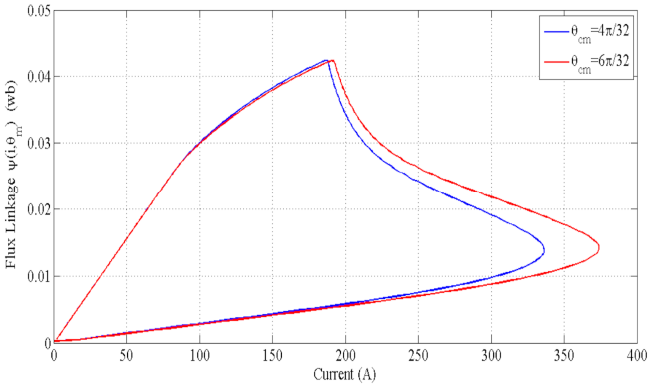

Fig.5. Estimated flux linkage loci at 32 krpm for different chamfer angles,-single voltage pulse operation, 270V; duration: 24º elect

The change-of-inductance period is thus 'elongated' and two different alignment periods, with two different gradients are introduced, ref. Fig.3. During the first period, the poles start overlapping but the increased reluctance due to the chamfer limits its positional-rate-of change. During the second period, starting at θ_{1cm}, the rotor crown starts to overlap in a similar fashion to the original non-chamfered designs. Thus, a similar positional-rate-of-change of inductance is experienced, with duration approximately equal to β_s. A number of effects need to be noted.

The first is a positive effect in that the introduction of such a chamfer widens the rotor slot at the air-gap, thus decreasing the unaligned inductance when compared to a similar non-chamfer design, ref. Fig.4, thus enabling higher torque production in the high-speed region as per Fig.5.

The second effect is however detrimental in the low-speed, high-torque region, in that the introduced chamfer increases the magnetic impedance when compared to the non-chamfered designs thus increasing stator pole leakage flux. Due to this increased reluctance, a slight reduction in the total flux handled by the circuit could be observed for identical current loading conditions. Such an effect lowers the positional rate-of-change of inductance even during the main-alignment period (which should ideally have the same gradient as the non-chamfered design). Thus, if not carefully catered for, the introduction of such a chamfer might bring about a reduction in the Torque/Ampere ratio of the machine.

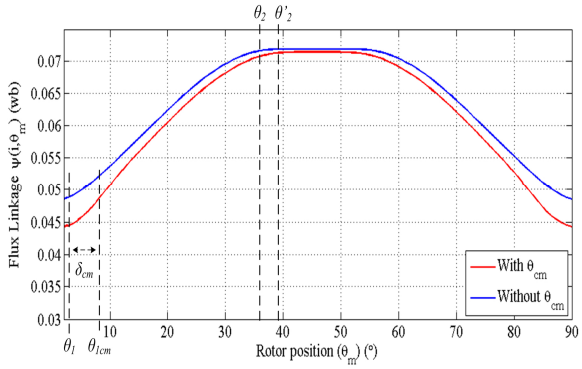

Fig.6. Plot showing the flux-linkage for the chamfered and non-chamfered designs at maximum current.

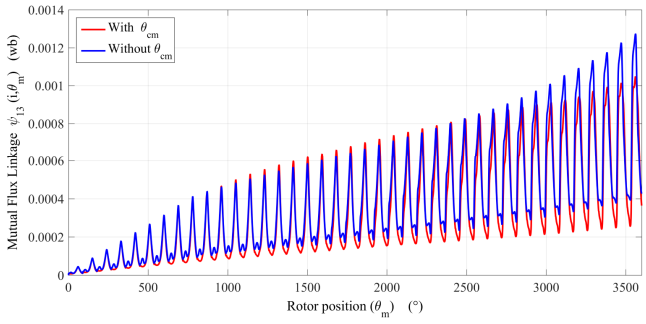

Fig.7. Plot showing mutual flux linkage with Phase 3 for the chamfered and non-chamfered designs

Both these effects can be observed in Fig.4 and Fig.6 which portray the self-flux linkage variation obtained via a 2D Finite Element (FE) profiling analysis for a sub-optimal design. During such 'quasi-static' evaluation the rotor was moved in discrete steps through one electrical revolution (90º mechanical) under constant current, single coil excitation. In this case, forty fixed current steps were considered until a phase current of 1000 A was reached. The FE suite used was Magnet™ from Infolytica©. The model employed 530,000 nodes and used a non-linear BH characteristic for the ferromagnetic materials considered, (Vacoflux48 for the stator and Vacodur S+ for the rotor).

The required initial magnetisation curves were provided by the material supplier Vacuumschmelze GmbH.

A third important effect of introducing such a chamfer is the effective control on the mutual flux contribution. This is of particular importance during current overlap where the mutual flux contribution holds the turning-off phase into saturation even though the current through it starts decreasing. This brings about a reduction in the aligned unsaturated inductance *Lau* and therefore a further reduction in the torque-developing potential of the phase. The reduction of such mutual flux contribution is shown for the same design in Fig.7.

The combined effect of the mentioned features resulted in a machine capable of operation at and above the given torque-speed envelope. The final design had stator and effective rotor pole arc angles at 30º and 41.75º respectively together with a pole chamfer angle of 8π/32.

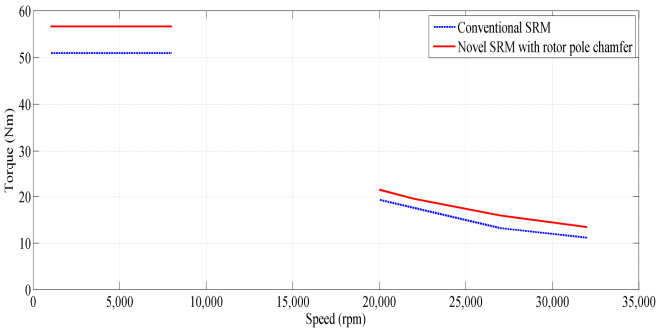

Fig.8. Comparison of simulated performance between proposed and conventional geometry machines

An initial Torque-speed characteristic comparison to a standard machine geometry (having conventional stator and rotor teeth and identical dimensions to the new design) was performed using a Simulink® based SRM block model with results reported in Fig.8. At low speeds, (up to 8000 rpm), the current was limited to 600A (nominal) via a hysteresis controller set at ±10% nominal current.

2) Rotor Structural evaluation

Further to the introduction of the described chamfer, two other features were added to the rotor profile. The first, described in [4] saw the introduction of a cavity within the rotor pole structure to increase its magnetic utilization as shown in Fig.2. With the correct sizing this feature reduced the rotor weight by 3.5% with minimal torque reduction (0.57%), at base speed.

The second feature allowed for the inclusion of rotor-slot inserts to render the whole structure more aerodynamically efficient. This required a minor modification in rotor-slot geometry to allow for their retention at such high speeds. The chosen material was a high temperature thermo-setting polymer, (μ_r=1), called Meldin7001, rated for continuous use at temperatures above 300˚C.

An optimization of the rotor geometry to reduce stress concentration issues and ensure its safe operation at the operating speed of 32krpm was thus carried out.

Due to the predominantly radial nature of the experienced forces, a 2D plane-stress model was setup within ANSYS® Workbench R15, an off-the shelf, FE suite. The model used 185873 nodes with 60249 elements of type Plane82 for the lamination geometry. A linear elastic behaviour was assumed for all materials, whilst allowing for large displacements, geometric non-linearities and thermally induced stresses. The thermal and centrifugal conditions were imposed on the complete body or bodies.

The rotor surface temperature was estimated at 300ºC using the thermal model similar to that described in [16] as detailed in [4] and correlations given in [17-19]. The input iron and copper losses are reported in Table I. Results for the undergone structural analysis in the 'Hot rotor' condition at nominal speed (32krpm) are reported in Fig.9.

Using the estimated stress distribution, the final laminate material was chosen to be VACODURS+ with a minimum proof stress of 750 MPa.

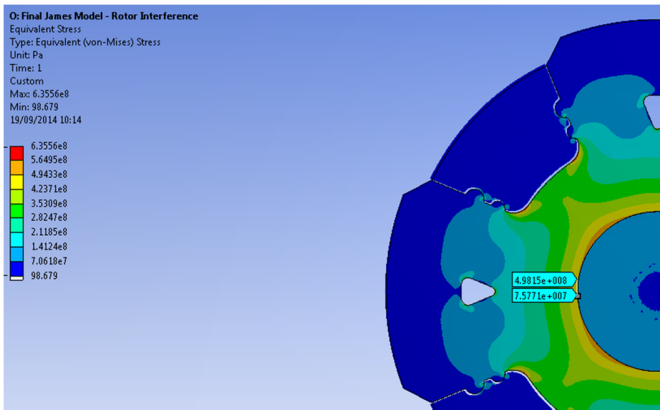

Fig.9. Equivalent Von Mises Stress distribution in the finalized rotor geometry at the peak estimated temperatures including inserts

At the imposed rotor temperatures, and rated speed, the peak deformation of the rotor pole at the air-gap was estimated at 0.24 mm whilst the Meldin deformed by a maximum of 0.7 mm. Such a large deformation was however allowed since the inserts' outer edge was purposely located at a smaller diameter than the air gap.

E. Simulated Drive performance summary

In order to better quantify the machine performance together with the incurred iron and switching losses, particularly for the low speed high torque region in which current control is provided via a hysteresis controller, a co-simulation approach was adopted based on a Matlab® Simulink® platform.

The required asymmetric H-bridge driving the SRM was modelled using a PLECS™ library for non-ideal Power-Electronic (PE) devices and controlled via a hysteretic current controller in Simulink®. This control environment was linked via a dedicated Simulink® block provided by the FE suite developer, Infolytica©. The PE losses included both conduction and switching loss terms, both of which were estimated using an off-the-self PLECS library model for IGBTs. Briefly the conduction losses were based on an equivalent IGBT model using a series connection of a DC voltage source, U_{ceo}, (representing the device on-state-zero-current collector-emitter voltage), and a collector-emitter on-state resistance , r_{ce}, values of which were read-off the respective datasheet and inputted to the model. The switching loss energies for both IGBT and diode (mainly reverse recovery energy during IGBT turn-on) were estimated using the datasheet reported energy loss, computed collector current and collector-emitter voltage. A fixed time interval had to be implemented for the FE-solving block to function correctly. The maximum simulation time-step was set to 1 ns.

Using this method, the simulated performance for the final drive design at three salient power-speed nodes was evaluated, proving the wide constant power speed range capability of the designed machine, ref. Table I. Note a worst-case switching-loss condition was assumed by imposing a switching strategy in which both top and bottom devices (ref. Fig.10) were turned-off simultaneously.

TABLE I
PERFORMANCE SUMMARY FOR THE FINAL DRIVE

Speed	Torque	Iron losses		Ohmic Losses/phase @ 180C	Current		Total factored Iron losses & Ohmic	Motor Efficiency	Switching losses Maximum	Total system Efficiency
		Stator	Rotor		Peak	Rms				
rpm	Nm	(W)	(W)	(W)	(A)	(A)	(W)	%	(W)	%
8000	56.3	437	1238	479	706	347	4787	90.79	3000	85.83
19200	26.1	738	1245	279	509	208	4803	91.61	1070	89.93
32000	15.77	1080	1765	132	414	167	6059	89.71	1000	88.22

III. THE POWER ELECTRONIC CONVERTER

The power electronic converter (PEC) chosen was of the full-asymmetric bridge type, the general layout of which is shown for a single phase in Fig.10. Such a topology was chosen in order to maintain complete phase decoupling and individual controllability [20-22].

During motoring operation, the converter effectively acts as a current source, with both top and bottom devices, Q1 and Q2, turning-on simultaneously allowing current to flow to the winding. In generation mode, the switches turn–on briefly to establish a linking field, (usually with poles in complete alignment) and open just as the poles start to part, allowing the harvested kinetic energy of the system to flow toward the DC-link via the diodes D1 and D2.

To reduce the switching losses during the motoring mode a toggle function was included in the control board design to allow for the alternate turn-off of Q1 and Q2. This function effectively reduces the switching frequency for each device by half. However, by so doing the available de-magnetizing voltage is also halved (detrimental for high speed operation), since at turn-off the coil terminals are shorted out via a diode to either one of the DC link connections. For this reason this feature could be enabled or disabled by the user at any time depending on the required current decay rate.

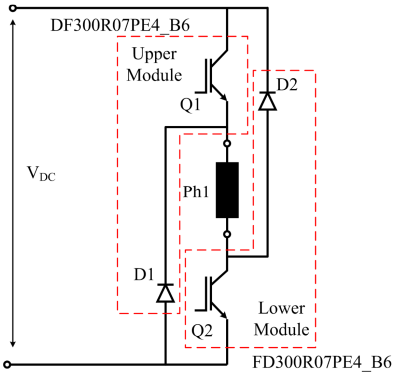

Fig.10. Power electronic topology for the built converter showing the chopper modules used.

Initial testing was carried out with such a feature disabled.

In order to handle the required peak current in excess of 600 A, a chopper module from Infineon was used for each switch making up the PEC. To cater for the designed converter asymmetry two types of modules were employed. Each module had, 3 separate ‘legs’ with one IGBT in series with a diode, both rated at 300 A. To meet the high peak current demand, the gate drive circuit was thus designed to drive all the three ‘legs’ making up one module, in parallel thus allowing for current pulses of up to 900 A peak.

A rate limiter was implemented, to protect the IGBTs, by introducing a minimum turn-off period duration of 25 µs. This feature was desirable during the low unaligned inductance periods where the machine’s electrical time constant is very low. However it reduced controllability of the phase current, with a variation of the set hysteresis band, occurring due to the overriding of the turn-on command issued by the current controller. This effect was noted during the performed testing.

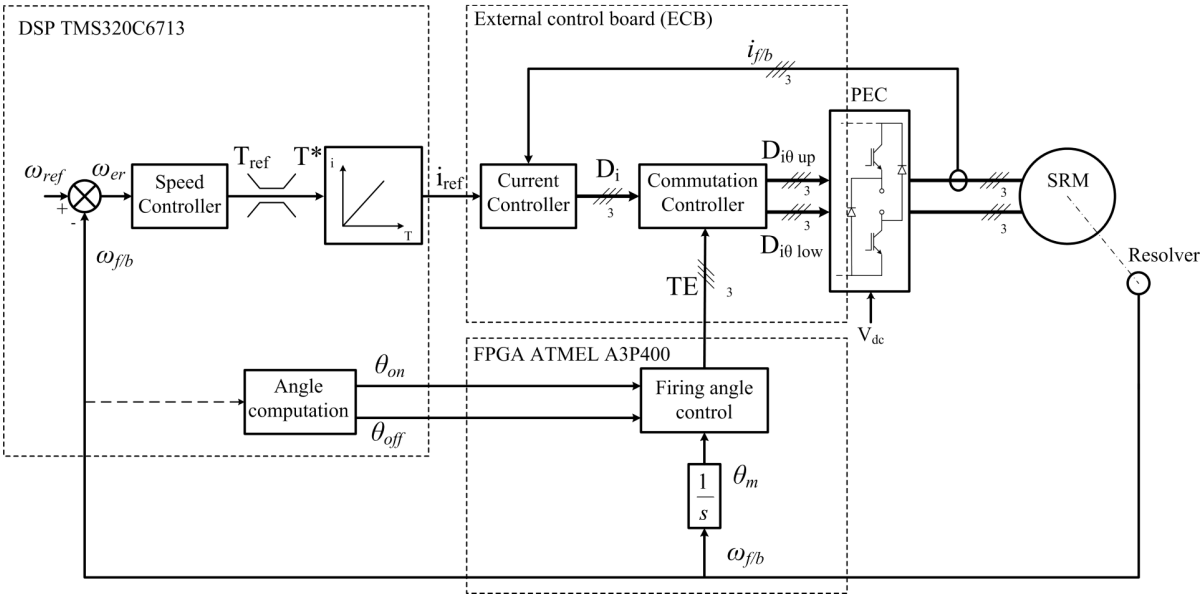

Fig.11. Control structure implemented

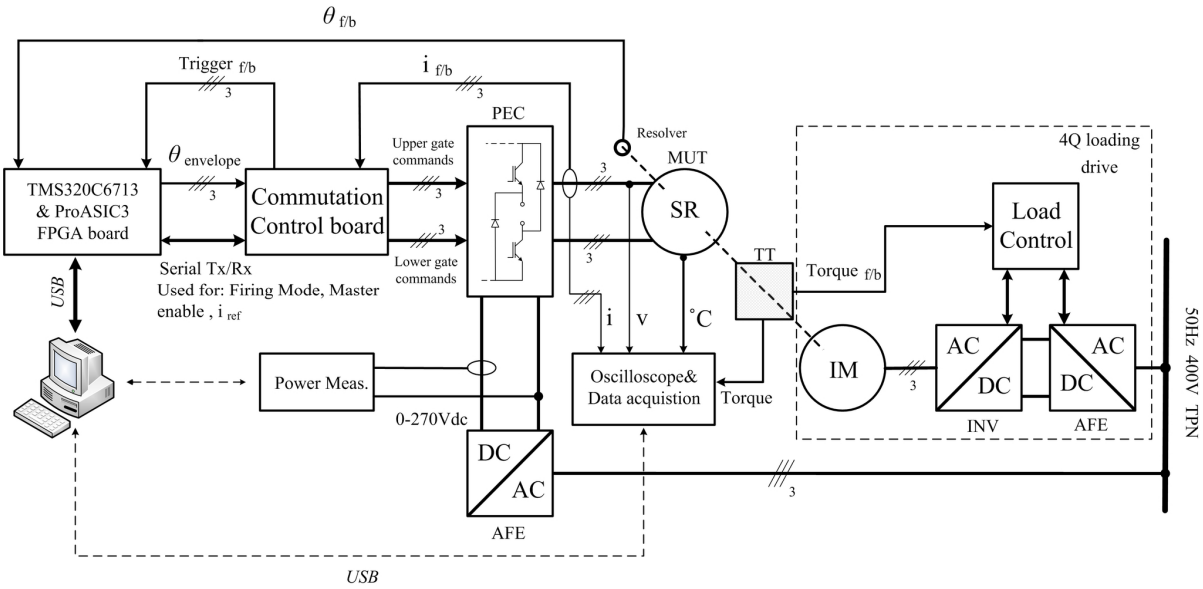

Fig.12. Schematic representation of the implemented test setup

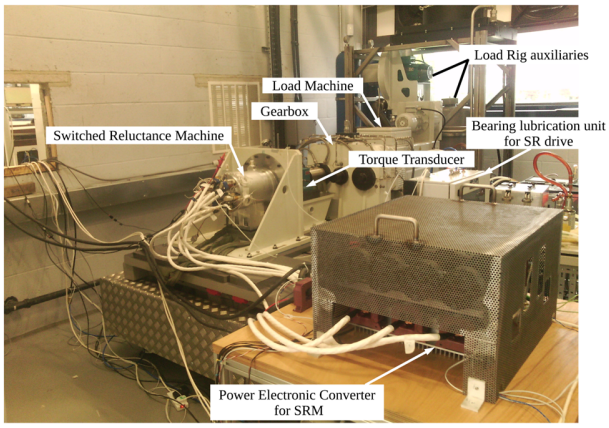

Fig.13. Photograph showing the implemented test-rig

IV. The Control Structure Used

For initial testing purposes a proportional integrator (PI) type speed controller was implemented as the drive's outermost control loop. The control routine was implemented on a TMS320C6713 DSP

It used a 225 MHz clock and was incorporated within a standalone development kit from Digital Spectrum® (DSK). The DSK was interfaced to an Actel™ Proasic3® FPGA, to generate the required gating signs as a function of angular positions as shown in Fig.11.

Further to this, using the performed simulations, over the motoring speed range (0-8 krpm), it was found that a linear relationship could be developed to relate the reference torque issued from the speed controller, to the desired current reference in agreement with [6].

V. The Test Setup

The built SRM was coupled to the loading induction motor (150 kW, 1480 rpm) via a 160 Nm torque transducer (type: ET1303 from Torquemeters® ltd.) and a speed- increasing gearbox having a ratio of 1:6.154, ref. Fig 12, 13.

During the constant speed load tests carried out, the load machine was operated in the Generator mode via the UNICO 2400-series 4-quadrant converter, which was set to operate the machine in torque-control mode. The SRM was operated in motoring mode (1st Quadrant) and controlled in speed-control mode via the implemented algorithm on the DSP-FPGA controller board.

VI. Results

A. Static tests

A set of initial machine tests were performed before its dynamic loading in which the flux linkage characteristic at various rotor positions were measured using a method highlighted in [23]. The measured flux linkage curves are reported and compared to those obtained at the design stage using FE solvers, in Fig.14.

As can be noted, the resultant ψ-i domain characteristics exhibit a very good agreement with those derived from FE analysis. This is particularly so for regions in which a high level of MMF is imposed by the windings on the constituent material. In these regions deviations noted were of the order of <5% from initial estimation. However larger discrepancies were noted in the low current regions for all curves which related to rotor positions in which the ferromagnetic nature of the magnetic circuit formed is dominant, i.e. for rotor angles greater than 10º (moving towards complete alignment, at 45º).

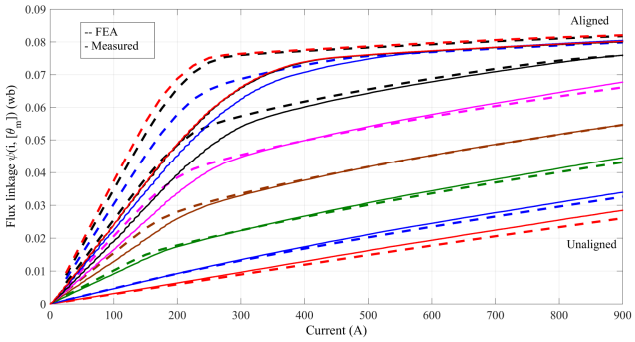

Fig.14. Comparison between measured and FEA flux linkage characteristics

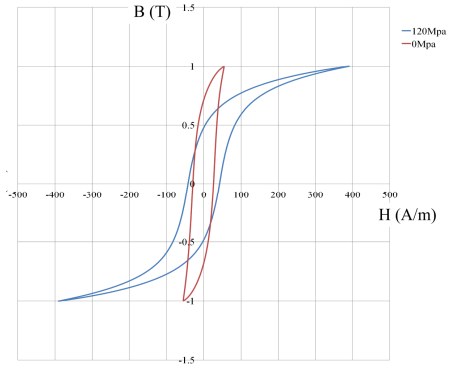

Fig.15. Effect on the BH curve at 1T 50Hz of Vacoflux48 when subjected to 120Mpa of compressive stress

Initial investigations into the noted discrepancy in the low-MMF pole-alignment regions of the ψ-i characteristic indicate that a contributing factor for such a drift was due to an underestimation of the degradation in magnetic properties of the constituent materials when subjected to compressive mechanical stresses, ref. Fig15.

Using a single sheet tester developed to allow for sample compression during loss measurement, it was found that the material's coercivity and required field strength to magnetise the sample of stator material, Vacoflux 48, varied drastically upon applying compressive loads similar to that experienced due to the housing's interference fit.

The noted shift is also in agreement with reported measurements under similar conditions, (different material) in [24].

TABLE II
PRELIMINARY RESULTS SHOWING IRON LOSS INCREASE FOR VACUFLUX48 UNDER COMPRESSIVE STRESS AT 120MPA

Induction T	Frequency Hz	Loss deviation %
1	400	+7.42
1	1000	+18.21
2	400	+43.84
2	1000	+52.62

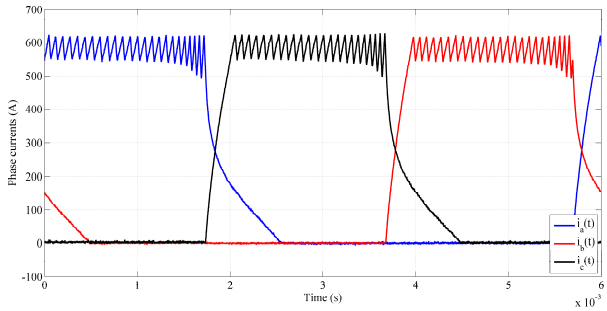

Fig.16. Current waveforms at 54.6 Nm, 2.5 krpm

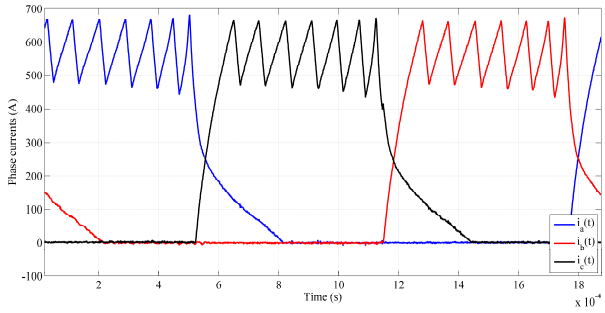

Fig.17.Current waveforms at 53.4 Nm, 8 krpm

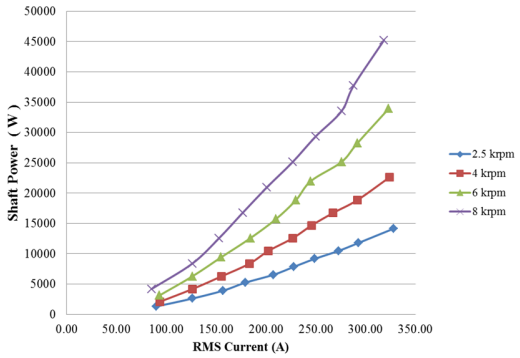

Fig.18. Output power vs measured current (RMS) at various speeds

Effectively such change increases the magnetic reluctance and hence reduces the flux-carrying capacity of the stator at low MMF values.

Preliminary results for the increase in iron-loss over the 0 MPa case for the identical stress level reported in Fig.15 are given in Table II. Continued investigations in this area are underway.

B. Constant speed tests

Initial testing with the machine running was carried out in motoring mode up to full torque at speeds varying from 2.5 to 8 krpm.

The measured phase current profiles at 2.5 krpm during heavy loading conditions are reported in Fig.16. Whilst the resulting current profiles, during the rated base-speed operation at 53.4 Nm and 8 krpm are shown in Fig.17.

The effect of imposing a minimum OFF-period can be noticed towards the end of the current profile in Fig 17.

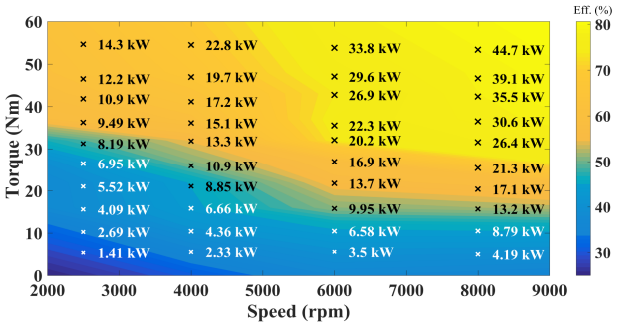

Fig.19. Torque-Speed-Power-Efficiency map for measured nodes.

At the instant mentioned, the current is allowed to drop beyond the established minimum, as the IGBTs remain turned off for the pre-set time. The developed shaft power against RMS phase current is given in Fig.18, whilst the measured torque-speed-efficiency map is given in Fig.19.

The efficiency of the developed drive, (excluding the cooling system), at the rated base speed operation was measured at 82%, which lies within 5% of the simulated, (drive-only), performance estimates presented in Table I for identical operating conditions.

VII. Conclusion

This paper described an SR machine designed for operation over a very wide (1:4) constant-power-speed-range using traditional discontinuous current control. The results presented are those measured during the initial testing phase. To the authors' knowledge, such capability was previously only possible via alternative control schemes such as that presented in [25].

Measured data prove that the machine is capable of reaching it base-speed performance at 53.4 Nm, 45 kW respectively. The associated density values were estimated at 11.62 Nm/ltr and 9.75 kW/ltr respectively.

Further to this, the results presented for the measured flux-linkage characteristic are in general agreement with the FE-model, however a previously unquantified source of error due to the constituent ferromagnetic materials' behaviour under mechanical stress was identified and further investigation proposed.

The measured efficiency of the developed drive, excluding the cooling system, at the peak torque conditions matched closely with the initially estimated figures at 82%.

Further test rig modifications are underway to improve machine-gearbox alignment and address other mechanical limitations of the employed loading rig in order to allow for higher-speed tests to be conducted.

References

[1] M.J. Provost "The More Electric Aero-Engine: A general Overview from an engine Manufacturer". *in IET Power Electronics Machines and Drives,Conference on, (PEMD), June 2002* .

[2] E. Ganev, "Selecting the Best Electric Machines for Electrical Power-Generation Systems", *IEEE Elect. Mag.* DOI *10.1109/MELE.2014.2364731 Dec.2014*

[3] J. Borg Bartolo, C. Gerada, "The Electromagnetic Design of a High Speed 45kW Switched Reluctance Machine having a Novel Rotor Geometry for Aerospace Application," in *Electrical Machines (ICEM) XXI International Conference on.,Berlin Sept.2014:*.

[4] J. Borg Bartolo, C. Gerada "Design and Modeling of a 45kW, Switched Reluctance Starter-Generator for a Regional Jet Application" in *SAE.Aerospace and Technology Conference (ASTC). Ohio Sept.2014*.

[5] S.R. MacMinn, W.D. Jones "A Very high speed Switched reluctance Starter generator for Aircraft Engine Applications" in *IEEE Aerospace and Electronics Conference (NAECON) proc. of.Dayton, May 1989*.

[6] C.A Ferriera, S.R Jones, W.S Heglund ,W.D. Jones,. "Detailed Design of a 30kW Switched Reluctance Starter Generator System for a Gas Turbine Engine Application".in *IEEE Trans. Ind.Appl. Vol 31 no.3, DOI:10.1109/28.382116 May/June 1995*

[7] S.Shoujun, L.Weiguo, D. Peitsch, U. Schaefer., " Detailed Design of a High Speed Switched Reluctance Starter/Generator for More/All Electric Aircraft". in *ELSEVIER Chinese Journal of Aeronautics, Vol 23. April 2009*

[8] R. Hall, A.G. Jack, B.C Mecrow, A.J Mitcham, "Design and intial testing of an Outer rotating segmented Rotor Switched Reluctance Machine for an Aero-Engine Shaft-line Embedded Stater/Generator" *IEEE Electric Machines and Drives Int. Conf. on, San Antonio, May2005*

[9] N.S Gameiro, A.J Marques Cardoso, "A new Method for Power Converter Fault Diagnosis in SRM Drives".*in IEEE Trans.Ind Appl.,Vol 48 no.2: pp. 653-662, March 2012*.

[10] T.J.E Miller,,"Converter Volt-Ampere Requirements of the Switched Reluctance Motor Drive". in *IEEE Trans. Ind. Appl., Vol. 1A no.5:pp 1136-1143; Sept. 1985*

[11] R. Krishnan, "Switched Reluctance Motor Drives Modeling, Simulation, Analysis, Design, and Applications", *1st ed. Ser: Ind. Elect., CRC press June 2001 ISBN: 9780849308383*.

[12] N. Schofield, S.A Long, D. Howe, M. McClelland, "Design of a Switched Relucatnce Machine for Extended Speed Operation"in *IEEE Trans. Ind. Appl.,Vol 45 no.1: pp. 116-122, Jan.2009*

[13] I. Husain, S.A. Hossain,"Modelling Simulation and COntrol of Switched Relucatance Motor Drives",in *IEEE Trans. Ind. Electron. Vol.52 no.6, pp1625-1634,Dec.2005*

[14] B.Bilgin, A. Emadi, M. Krishnamurthy, "Design Considerations for Switched Reluctance Machines With a Higher Number of Rotor Poles"in *IEEE Trans. Ind. Electron. Vol.59 no.10, pp.3745-3756, Oct. 2012*

[15] J.M. Stephenson, J. Corda, "Computation of torque and current in doubly salient reluctance motors from nonlinear magnetisation data" in. *Proceedings of IEE, Vol 126 no.5, May 1979.*

[16] D. Gerada, D. Borg-Bartolo, A. Mebarki,C. Micallef, N.L Brown, C. Gerada," Electrical machines for high speed applications with a wide constant-power region requirement" in *Electric Machines and Systems, (ICEMS) Intl. Conf. on Beijing, Aug. 2011*.

[17] D.A Howey, P.R.N Childs, A.S Holmes; "Air-Gap Convection in Rotating Electrical Machines" in *IEEE Trans. Ind. Electron. Vol.59 no.3, March 2012*

[18] D.A. Staton, A. Cavagnino; "Convection Heat Transfer and Flow Calculations Suitable for Electric Machines Thermal Models" in *IEEE Trans.Ind. Electron. Vol.55 no.10, Oct.2008*

[19] A. Boglietti, A. Cavagnino, D. Staton," Determination of Critical Parameters in Electrical Machine Thermal Models" in *IEEE Trans. Ind. Appl.,Vol 44 no.4: pp. 1150-1160, July.2008*

[20] S. Vukosavic, V. Stefanovic, "SRM inverter topologies: a comparative evaluation" in *IEEE Trans. Ind. Appl.,Vol 27 no.6:Dec 1991*

[21] R. Krishnan, P.N. Materu, "Design of a single-switch-per-phase converter for switched reluctance motor drives" in *IEEE Trans. Ind. Electron. Vol.37 no.6, Dec 1990*

[22] N.H. Fuengwarodsakul, M. Menne, R.B. Inderka; R.W. De Doncker,."High-dynamic four-quadrant switched reluctance drive based on DITC"in *IEEE Trans. Ind. Appl.,Vol 41 no.5: Sept.2005*

[23] P. Zhang , A. Cassini , S. Williamson, "An Accurate Inductance Profile Measurement Technique for Switched Reluctance Machines"in *IEEE Trans.Ind. Electron. Vol.57 no.9, Sept 2010.*

[24] L. Bernard, X. Mininger, L Daniel, G. Krebs, F. Bouillault, M.Gabsi, "Effect of Stress on Switched Reluctance Motors: A Magneto-Elastic Finite-Element Approach Based on Multiscale Constitutive Laws" in *IEEE Trans. on Mag, Vol.47 no.9: pp 2171-2178, April 2011*

[25] H. Hannoun, M. Hilairet, C. Marchand, "Design of an SRM Speed Control Strategy for a Wide Range of Operating Speeds" in *IEEE Trans.Ind. Electron. Vol.57 no.9, Sept 2010*

James Borg Bartolo was born in Malta in 1983. He received his B.Eng. (Hons.) and M.Phil. Degrees in electrical engineering from the University of Malta in 2005 and 2008 respectively. In 2011 he joined the University of Nottingham as PhD student with particular focus on high performance switched reluctance drives for transport applications. In March 2016 he received his PhD degree in Electrical and Electronic Engineering.

He has previously worked in the power generation sector, the University of Nottingham and is currently employed as Research and Development engineer at maxon motor AG, Switzerland where he is responsible with others for the development of novel motor drives. His main research interests lie in high performance electrical machines and iron loss measurement.

Marco Degano (M'03) received the 5 years Laurea Degree in Electronic Engineering from the Universita' degli studi di Udine (Italy) in April 2004. In February 2008 he joined the University of Nottingham as a visiting research fellow within the Marie Curie program. In October 2012 he received his PhD degree in Electrical and Electronic Engineering.

He is currently a research fellow with the Power Electronics Machines and Drives (PEMC) group at the University of Nottingham. His current research interests are in the fields of power electronic converters with particular focus on aerospace applications.

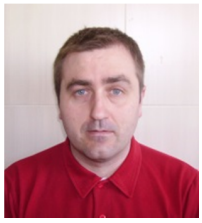

Jordi Espina received the M. Eng and PhD degrees from the Universitat Politècnica de Catalunya (UPC), Catalonia, Spain, in 2005 and 2011 respectively.

He is currently a Research Fellow with Power Electronics Machines and Control group (PEMC) at the University of Nottingham. His research interests are variable-speed drive systems, EMC, power electronics converters and integration on power electronics

Chris Gerada (M'05) received the Ph.D. degree in numerical modelling of electrical machines from The University of Nottingham, Nottingham, U.K., in 2005.

He subsequently worked as a Researcher with The University of Nottingham on high-performance electrical drives and on the design and modelling of electromagnetic actuators for aerospace applications. Since 2006, he has been the Project Manager of the GE Aviation Strategic Partnership. In 2008, he was appointed as a Lecturer in electrical machines; in 2011, as an Associate Professor; and in 2013, as a Professor at The University of Nottingham. His main research interests include the design and modelling of high-performance electric drives and machines.

Prof. Gerada serves as an Associate Editor for the IEEE TRANSACTIONS ON INDUSTRY APPLICATIONS and is the Chair of the IEEE IES Electrical Machines Committee